CHAPTER 5

DNA / protein binding and magnetic properties of a 1D Cu(II) complexes containing fumarate/terephthalate and Schiff base ligands

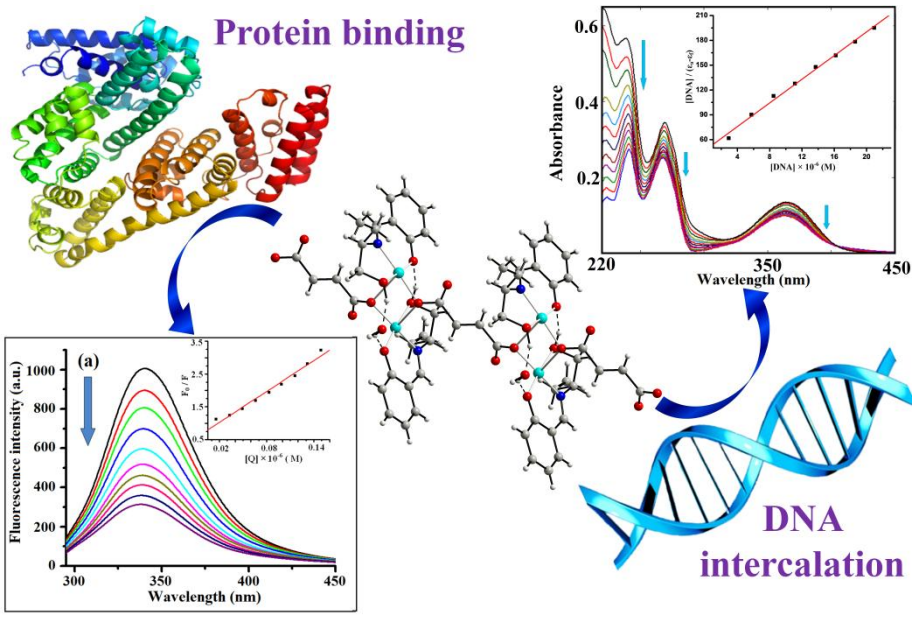

A. Paul et al. / Polyhedron 119 (2016) 460-470

5.1 **Introduction**

The design and synthesis of polynuclear metal complexes have become and active area of research for the last few decades due to their interesting molecular structure, crystal packing and potential application in the field of magnetism [5.1], fluorescence [5.2], catalysis [5.3] and bio-inorganic chemistry [5.4]. The choice of ligands is one of the important factors for designing such polynuclear metal complexes. Chelating organic ligands block some coordination sites of the metal ions, whereas organic spacers serve to link the metal ions and form polynuclear metal complexes [5.5]. Multidentate flexible Schiff bases are often used to build polynuclear complexes, since they can efficiently block some coordination sites of metal ions [5.6]. The use of Schiff base in combination with the linear dicarboxylate is an important strategy for synthesis of polynuclear complexes and in this combination the Schiff bases function as chelating ligand and linear dicarboxylate behaves as spacer [5.7]. Among the 3d metal ions, the polynuclear chemistry of Cu(II) is very important since it exhibits a rich variety of coordination geometries e.g., tetragonal, tetrahedral, square planar, trigonalbipyramidal etc. and hence prediction of final structure and molecular topology of polynuclear copper (II) compounds are difficult [5.8]. In addition to their noble structures / geometries, the copper compounds show interesting magnetic properties [5.9], anticancer activity [5.10] and bio-inorganic modeling [5.11].

Fumaric acid (H_2fum) and terephthalic acid (H_2tp), possesses versatile coordination mode and have special conformation with a 180° angle between the carboxylic acid groups. Both acids can function as mediator for transmitting the exchange interaction between the paramagnetic metal centers [5.12]. Since the metal-metal distance through the fum^{2-} and tp^{2-} ligands are above 9.2 Å, the bridging spacer does not effectively transmit magnetic exchange, however fum^{2-} sometime

exhibit monoatomic bridging mode and function as mediator for ferromagnetic exchange interaction [5.13].

Literature survey reveals that many copper(II) based coordination compounds are used as metallo-pharmaceuticals [5.14] and these compounds play important role in biology due to their antimicrobial [5.15], antifungal [5.16], antibacterial [5.17], antitumoral [5.18], antiviral [5.19], antipyretic [5.16a] and antidiabetic activities [5.20a]. The study of the interaction of copper(II) compounds with DNA under physiological conditions is important for the design of copper(II) based new pharmaceuticals. On the other hand, serum albumin is most abundant soluble protein in the circulatory system and function as transporter and disposer of pharmaceuticals [5.20b]. For this reason the analysis of kinetics of the interaction of DNA / serum albumins and copper complex is important to determine the affinity of copper complex to DNA / protein, and this information will promote the development of copper metal based efficient metallopharmaceuticals.

(E)-2-((1-hydroxybutan-2-ylimino)methyl)phenol (H_2L^1) and [(E)-2-((1-hydroxybutan-2-ylimino)methyl)-6-methoxyphenol] (H_2L^2) are potential polydentate Schiff bases for the synthesis of 3d metal coordination compounds and using these ligands some copper(II) and Ni(II) compounds have been reported in the literature [5.21]. However, to date there have been no report on 1D coordination polymeric compounds using these ligands. To synthesize coordination polymeric compound, we have adopted a synthetic strategy where linear dicarboxylate is used in combination with the above Sciff bases.

In the present contribution we have used alkoxo, hydroxo, phenoxo and imine donor Schiff bases [(E)-2-((1-hydroxybutan-2-ylimino)methyl)phenol] (H_2L^1) and [(E)-2-((1-hydroxybutan-2-ylimino)methyl)-6-methoxyphenol] (H_2L^2) and synthesized two 1D polynuclear copper(II)

compounds$\{[Cu_2(HL^1)_2(fum)]\cdot(H_2O)\cdot(MeOH)\}_n$ (**1**) and $\{[Cu_2(L^2)_2(tp)]\cdot(H_2O)\}_n$ (**2**) (fum = fumarate; tp = terephthalate). The kinetics of interaction of complexes with calf thymus DNA (CT-DNA) and bovine / human serum albumins have been studied.

5.2 Experimental

5.2.1 Materials and physical measurements

High purity 2-amino-1-butanol was purchased from the Aldrich Chemical Co. Inc. and used as received. All other chemicals used were of analytical grade. Solvents used for spectroscopic studies were purifies and dried by standard procedures before use [5.22].

Elemental analyses (carbon, hydrogen and nitrogen) were performed using a Perkin-Elmer 240C elemental analyzer. IR spectra were recorded as KBr pellets on a Bruker Vector 22FT IR spectrophotometer operating from 400 to 4000 cm^{-1}. Electronic absorption spectra were obtained with Shimadzu UV-1601 UV-vis spectrophotometer at room temperature. Quartz cuvettes with a 1 cm path length and a 3 cm^3 volume were used for all measurements. Emission spectra were recorded on a Hitachi F-7000 spectrofluorimeter. Room temperature (300 K) spectra were obtained in methanolic solution using a quartz cell of 1 cm path length. The slit width was 2.5 nm for both excitation and emission.

The fluorescence quantum yield was determined using phenol as a reference and methanol medium for both complexes and reference. Emission spectra were recorded by exciting the complex and the reference phenol at the same wavelength, maintaining nearly equal absorbance (~ 0.1). The area of the emission spectrum was integrated using the software available in the instrument and the quantum yield calculated [5.23] according to the following equation:

$$\Phi_s = \Phi_r \frac{A_s}{A_r} \frac{I_r}{I_s} \frac{\eta_s^2}{\eta_r^2}$$

where Φ_s and Φ_r are the fluorescence quantum yield of the sample and reference, respectively. A_s and A_r are the respective optical densities at the wavelength of excitation, I_s and I_r correspond to the areas under the fluorescence curve; and η_s and η_r are the refractive index values for the sample and reference, respectively.

Temperature-dependent molar susceptibility measurements of polycrystalline sample was carried out at the *Servei de Magnetoquímica* of the Centres Científicsi Tecnològicsat the Universitat de Barcelona in a Quantum Design SQUID MPMSXL susceptometer with an applied field of 3000 and 198 G in the temperature ranges 2-300 and 2-30 K, respectively.

5.2.2 Synthesis of ligands

Multi-dentate Schiff base ligands [(E)-2-((1-hydroxybutan-2-ylimino)methyl)phenol] (H_2L^1) and [(E)-2-((1-hydroxybutan-2-ylimino)methyl)-6-methoxyphenol] (H_2L^2) were prepared by refluxing 1:1 mixture of 2-aminobutanol and corresponding aldehyde in methanol according to the chapter-2.

5.2.3 Synthesis of complexes

$\{[Cu_2(HL^1)_2(fum)]\cdot(H_2O)\cdot(MeOH)\}_n$ (1)

A methanolic solution (10 mL) of mixture of HL (1 mmol, 0.193 g) and triethylamine (TEA) (1 mmol) was added to a methanolic solution (10 mL) of $Cu(ClO_4)_2\cdot 6H_2O$ (1.0 mmol, 0.371 g), followed by stirring for 2h. To the resulting green mixture an aqueous solution (1 mL) of disodium fumarate (1mmol, 0.16 g) was added dropwise and resulting deep green reaction mixture was stirred for an additional 1h at 27°C, then filtered. The filtrate was kept in air for slow evaporation at room temperature. Deep green needle shaped single crystals suitable for X-ray diffraction were obtained by slow evaporation of methanolic solution after a few days. Yield: 78 %. *Anal.*Calc. for $C_{27}H_{36}Cu_2N_2O_{10}$ (675.66): C, 47.99; H, 5.37; N, 4.14%. Found: C,

48.50; H, 4.99; N, 4.37 %. IR (cm^{-1}): 3200-3600 (br, vs), 2982 (w), 1642 (s), 1552 (vs), 1468 (s), 1416 (vs), 1374 (s), 1302 (vs), 1244 (vw), 1196 (vw), 1082 (vw), 1021 (vw), 888 (vw), 691 (br, vw).

$\{[Cu_2(L^2)_2(tp)]\cdot(H_2O)\}_n$ (2)

Complex **2** was synthesized adopting the same procedure as for **2** using disodium terephthalate (1 mmol, 0.210 g) instead of disodium fumarate. Green crystals suitable for X-ray analysis were obtained from the filtrate. Yield: 77%. *Anal.*Calc. for $C_{32}H_{36}Cu_2N_2O_{11}$ (751.71): C, 51.12; H, 4.82; N, 3.72 %. Found: C, 51.03; H, 4.54; N, 3.75(%). IR (cm^{-1}): 3429 (vs), 2983 (w) 1644 (vs), 1552(vs), 1467 (s), 1414 (vs), 1373 (s), 1299 (s), 1245 (w), 1218 (vw), 1079 (s), 975 (w), 882(vw), 781 (vw), 635 (vw).

5.2.4 **Crystallographic data collection and refinement**

The crystal data of complex **1** was collected at room temperature using a Nonius Kappa CCD diffractometer with graphite monochromated Mo-Kα radiation. The data set was integrated with the Denzo-SMN package [5.24] and corrected for Lorentz, polarization and absorption effects (SORTAV) [5.25], whereas X-ray single crystal structural data of **2** was collected on a Bruker D8 Venture PHOTON 100 CMOS diffractometer equipped with a INCOATEC micro-focus source operating at 50 kV and 30 mA with graphite monochromated MoKα radiation, the program SAINT [5.26] was used for integration of diffraction profiles and absorption correction was applied with SADABS program [5.27]. The structure of **1** and **2** were solved by direct methods using SIR97 [5.28] and SIR92 [5.29] system of programs, respectively. The structure of **1** was refined using full-matrix least-squares with all non-hydrogen atoms anisotropically and hydrogens included on calculated positions, riding on their carrier atoms, except the hydrogen atoms forming H-bonds which were refined isotropically. The methyl group C26-H_3 was found

disordered and refined isotropically over two positions with occupancies of 0.6 and 0.4, respectively. The structure displays large voids occupied by disordered solvent molecules of Methanol. The O-H group, O9-H, was found disordered and the oxygen was refined anisotropically over two independent positions with occupancies of 0.6 and 0.4, respectively. All calculations were performed using SHELXL-2014/17 [5.30], PARST [5.31] and PLATON [5.32] implemented in WINGX [5.33] system of programs. Packing diagrams were done with graphical program Diamond [5.34]. Crystallographic data has been deposited at the Cambridge Crystallographic Data Centre and allocated the deposition numbers CCDC1476311 and CCDC1828394. The crystal data and details of structure refinement are given in Table 1.

Table 5.1 Crystal Data and Structure Refinement for complexes **1-2**

Complex	**1**	**2**
Empirical formula	$C_{27}H_{36}Cu_2N_2O_{10}$	$C_{32}H_{34}Cu_2N_2O_{11}$
Formula mass, g mol^{-1}	675.66	749.69
Crystal system	Monoclinic	Monoclinic
Space group	*P* $2_1/n$	*Pn*
a, Å	8.4944(3)	9.962(5)
b, Å	13.2905(4)	17.231(5)
c, Å	26.3919(9)	10.455(5)
α, deg	90	90
β, deg	96.916(1)	114.469(5)
γ, deg	90	90
V, $Å^3$	2957.8(2)	1633.5(12)
Z	4	2
$D_{(calcd)}$, g cm^{-3}	1.517	1.524
μ(Mo-Kα), mm^{-1}	14.95	1.365
F(000)	1400	772
Theta range, deg	3.07-25.50	2.4-28.4
No. of collected data	15779	67078
No. of unique data	5472	8152
R_{int}	0.0770	0.056
Observed reflns [$I > 2\sigma(I)$]	3504	7209
Goodness of fit (F^2)	1.076	1.032

Parameters refined	407	428
$R1$, $wR2$ $(I > 2\sigma(I))$ [a]	0.0695, 0.1593	0.0320, 0.0749
Residuals, e Å^{-3}	-0.540, 0.535	-0.25, 0.36

[a] $R1(Fo) = \Sigma \left| \left| Fo \right| - \left| Fc \right| \right| / \Sigma \left| Fo \right|$, $wR2(Fo^2) = [\Sigma w (Fo^2 - Fc^2)^2 / \Sigma w (Fo^2)^2]^{½}$

5.2.5 Albumin binding studies

Stock solutions of human serum albumin (HSA) and bovine serum albumin (BSA) were prepared in HEPES buffer (pH 7.2) solution. Aqueous solution of the copper(II) compounds were prepared by dissolving the compound in water : HEPES buffer (1:99). The interactions of compounds with serum albumins were studied by recording room temperature tryptophan fluorescence of HSA / BSA at 340 nm. Fluorescence spectra were recorded in the range 290-450 nm at an excitation wavelength of 280 nm. To the solutions of serum albumins, copper(II) compounds were added and the quenching of emission intensities at 340 nm (λ_{ex}, 280 nm) were recorded after incremental addition of aqueous solution of compounds. The Stern-Volmer constant (K_{sv}) and quenching rate constant (k_q) were calculated using the equations $F_0/F = 1 + K_{sv}$ [complex] and $K_{sv} = k_q\tau_0$, where F_0 and F are the fluorescence intensities in the absence and in the presence of the complex, and τ_0 is the lifetime of serum albumin (~ 5×10^{-9} s) [5.35]. To calculate the binding constant of the compound with SA, following Scatchard equation [5.36] have been used,

$$\log[(F_o - F)/F] = \log K_b + n \log[\text{complex}]$$

where K_b is the binding constant of the compound with serum albumin and n is the number of binding sites per albumin.

5.2.6. DNA binding experiments

Electronic absorption spectral study

UV-vis absorption spectroscopic technique has been used to investigate the possible binding mode and to calculate the intrinsic binding constant (K_{ib}) for the interaction of the compound with CT-DNA. Electronic absorption spectral titration was carried out at a fixed concentration of copper(II) compound in water and varying the concentration of CT-DNA. Intrinsic binding constant (K_{ib}) of the complex with CT-DNA was determined using the equation [5.37]

$$\frac{[DNA]}{(\varepsilon_a - \varepsilon_f)} = \frac{[DNA]}{(\varepsilon_b - \varepsilon_f)} + \frac{1}{K_{ib}(\varepsilon_b - \varepsilon_f)}$$

where, [DNA] is the concentration of CT-DNA, ε_a is the extinction co-efficient of the complex at a given CT-DNA concentration, ε_f and ε_b are the extinction co-efficient of the complex, in free solution and when fully bound to CT-DNA, respectively. The plot of $[DNA]/(\varepsilon_a-\varepsilon_f)$ versus [DNA] gives a straight line with $1/(\varepsilon_b-\varepsilon_f)$ and $1/[K_{ib}(\varepsilon_b-\varepsilon_f)]$ as slope and intercept, respectively. From the ratio of the slope to the intercept the value of K_{ib} could be calculated.

Competitive binding fluorescence measurement

The competitive binding nature of ethidium bromide (EB = 3,8-diamino-5-ethyl-6-phenyl phenanthridinium bromide and copper(II) compound, with CT-DNA was investigated adopting fluorometric method using aqueous solution of EB bound CT-DNA in HEPES buffer (pH 7.2) at room temperature. In presence of CT-DNA, ethidium bromide (EB) exhibits fluorescence enhancement due to its intercalative binding to DNA. Competitive binding of copper(II) compound with CT-DNA results fluorescence quenching due to displacement of EB from CT-DNA. The fluorescence intensities at 612 nm (λ_{ex}, 500 nm) of EB bounded CT-DNA with increasing concentration of copper(II) compound was recorded. The Stern-Volmer constant (K_{sv}) was calculated using Stern-Volmer equation [5.23] $F_0/F = 1 + K_{sv}[complex]$, where F_0 and F are

the emission intensities in absence and in presence of copper(II) compound, K_{sv} is the Stern-Volmer constant, and [complex] is the concentration of copper (II) compound.

5.3 Results and discussion

5.3.1 Crystal structure description

Molecular structure of $\{[Cu_2(HL^1)_2(fum)]\cdot(H_2O)\cdot(MeOH)\}_n$ (1)

Complex **1** crystallizes in the monoclinic system with space group $P2_1/n$. Crystallographic data and selected bend lengths and bond angles are depicted in Tables 5.1 and 5.2. The ORTEP [5.38] view of the asymmetric unit and the polymeric structure of complex **1** are shown in Figs. 5.1 and 5.2. The crystal structure analysis complex **1** shows that the $Cu_2(HL^1)_2$ units are connected by fumarate spacer, beside the presence of lattice water and methanol molecules. The crystallographic independent unit contains two copper(II) cation, two deprotonated Schiff base $(HL)^-$, one fumarate, one lattice water and one lattice methanol molecule. Copper atoms of asymmetric unit are again connected with fumarate and form ID polymeric structure (Fig. 5.2).

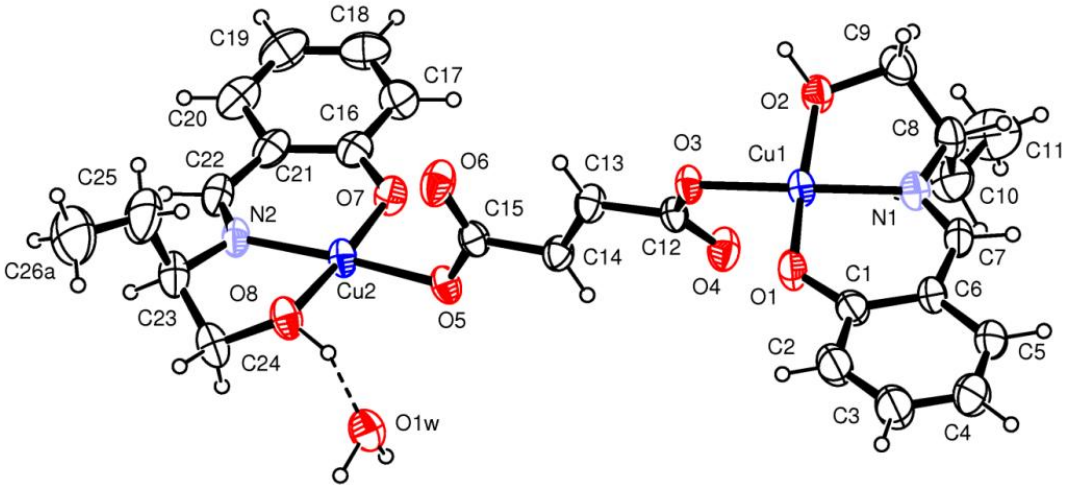

Fig. 5.1 ORTEP view of the asymmetric unit of complex **1** showing the thermal ellipsoids at 30% probability level.

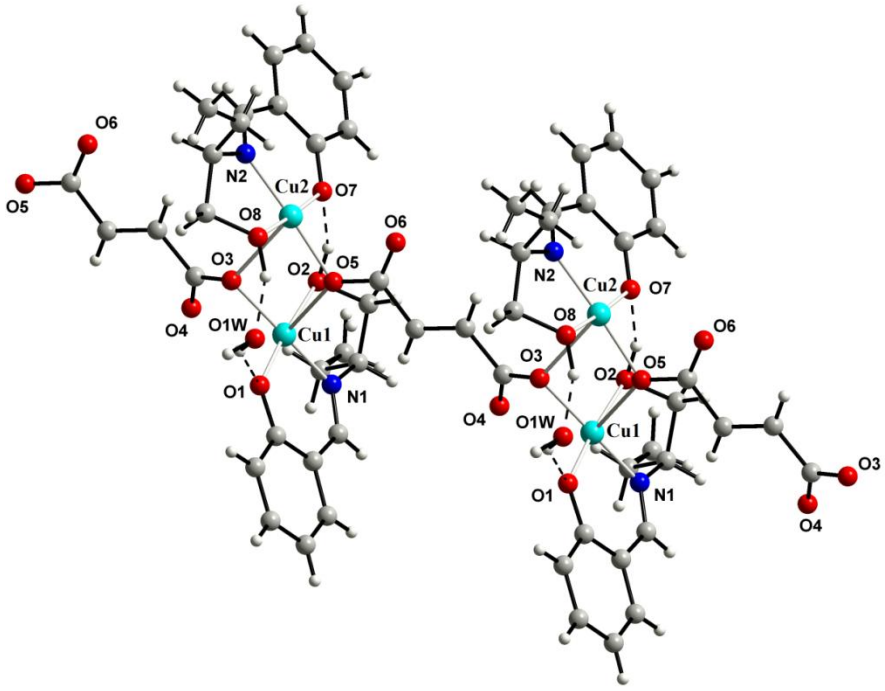

Fig. 5.2 The polymeric structure of complex **1** determined by the Cu1…O5 and Cu2…O3 interactions.

The coordination polyhedron for each metal is best described as slightly distorted square pyramidal geometry [trigonality τ_5 parameters [5.39] are 0.128 and 0.013 for Cu(1) and Cu(2), respectively]. The basal plane is occupied by the chelating tridentate Schiff base donors atoms [O(1), N(1), O(2) for Cu(1) and O(7), O(8), N(2), for Cu(2)] and by the fumarate oxygen donors [O(3) and O(5) for Cu(1) and Cu(2), respectively]. The apex of the square pyramid occupied by another fumarate oxygen at relatively longer distance [Cu(1)-O(5)' 2.384(4) Å; Cu(2)-O(3)'' 2.476(4) Å (Table 5.2)].

Table 5.2 Selected bond distances (Å) and angles (°) of complex **1**

Bond distances			
Cu(1)-O(1)	1.909(4)	Cu(2)-O(5)	1.943(4)
Cu(1)-O(2)	2.049(4)	Cu(2)-O(7)	1.912(4)
Cu(1)-O(3)	1.948(4)	Cu(2)-O(8)	1.994(4)
Cu(1)-N(1)	1.927(5)	Cu(2)-N(2)	1.936(5)
Cu(1)-O(5)'	2.384(4)	Cu(2)-O(3)''	2.476(4)

Bond angles			
O(1)-Cu(1)-O(2)	174.57(18)	O(7)-Cu(2)-O(8)	176.25(19)
O(1)-Cu(1)-O(3)	94.28(18)	O(7)-Cu(2)-O(5)	89.93(18)
O(1)-Cu(1)-N(1)	95.00(2)	O(7)-Cu(2)-N(2)	94.40(2)
O(1)-Cu(1)-O(5)'	94.62(16)	O(7)-Cu(2)-O(3)''	92.40(16)
O(2)-Cu(1)-O(3)	89.32(17)	O(8)-Cu(2)-O(5)	93.15(18)
O(2)-Cu(1)-N(1)	82.20(2)	O(8)-Cu(2)-N(2)	82.50(2)
O(2)-Cu(1)-O(5)'	82.10(16)	O(8)-Cu(2)-O(3)''	90.41(16)
O(3)-Cu(1)-N(1)	166.72(2)	O(5)-Cu(2)-N(2)	175.62(2)
O(3)-Cu(1)-O(5)'	78.50(14)	O(5)-Cu(2)-O(3)''	76.28(14)
N(1)-Cu(1)-O(5)'	110.21(18)	N(2)-Cu(2)-O(3)''	102.96(18)

Symmetry operations: (') at x+1,y,z and ('') at x-1, y, z

The copper atoms are displaced by 0.0363 and 0.013 Å for Cu(1) and Cu(2), respectively, from their basal planes. The basal coordination Cu-O bond distances are varying in the range 1.909(4) - 2.049(4) Å and 1.912(4) - 1.994(4) Å for Cu(1) and Cu(2), respectively whereas the apical Cu-O bonds are 2.384(4) and 2.476(4) Å for Cu(1) and Cu(2), respectively. The cisoid bond angles ranges from 78.50(14) to 110.21(18)° and 76.28(14) to 102.96(18)° for the Cu(1) and Cu(2) centers, respectively. On the other hand, the transoid bond angles are 166.72(2)°, 174.57(18)° (for Cu(1)), and 175.62(2)°, 176.25(19)° (for Cu(2)). The Cu(1)…Cu(2) separation in the carboxylato oxygen bridged dinuclear unit is 3.387Å. The packing diagram indicates that complex **1**exists as 1D polymeric chain through fumarate linkages, where Cu…Cu separations are 8.993Å and 9.294Å. A weak coordinative interaction between the Cu(1) and O(4) atoms [Cu(1)-O(4), 2.770 Å] also exists in the 1D chain. The 1D polymeric chains are involve in strong π…π interactions (Fig. 5.3) (centroid to centroid distance 3.66 Å, Table 5.3) and this results in 2D supramolecular sheets. Two such different 2D sheets are further connected with C-H…π interactions [5.40] (C-H…π (ring), 3.004 Å) to form a 3D supramolecular network (Fig. 5.4).

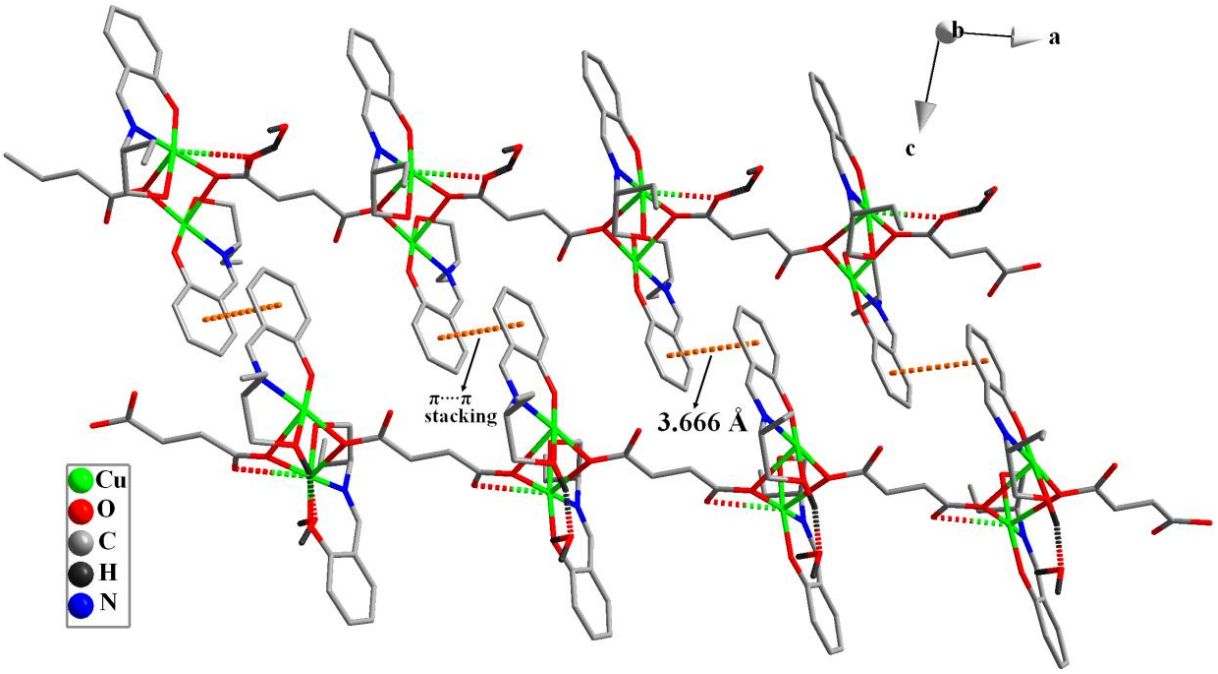

Fig. 5.3 2D supramolecular sheet of complex **1** formed with π…π interactions.

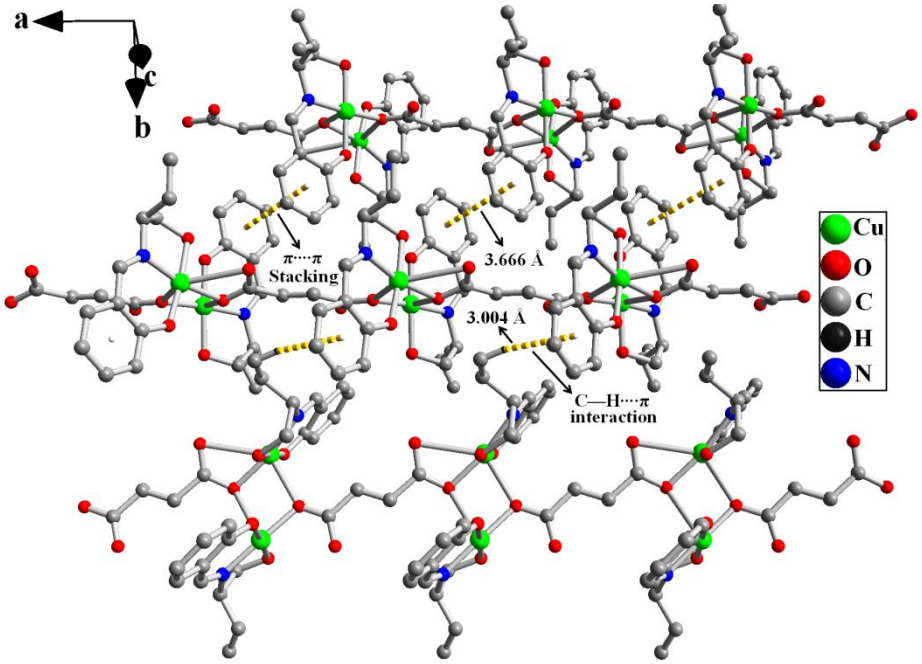

Fig. 5.4 3D supramolecular structure of complex **1** formed with π…π and C-H…π interactions.

Table 5.3. π…π interaction in complex **1**.

$C_{gi}\cdots C_{gj}$	Symmetry	d_{cc} (Å)	α (°)	β (°)	d_{cv} (Å)
Cg(14)···Cg(14)	-1-x, -y, 1-z	3.665(5)	0	17.82	-3.490(3)

Cg(14) → C(16)-C(17)-C(18)-C(19)-C(20)-C(21)
d_{cc} = Centroid-centroid distance between ring i and ring j.
d_{cv} = Vertical distance from ring centroid i to ring plane j.
α = Dihedral angle between the first ring mean plane and the second ring mean plane of the partner molecule.
β = Angle between centroids of first ring and second ring mean planes.

Molecular structure of $\{[Cu_2(L^2)_2(tp)]\cdot(H_2O)\}_n$ (2)

Complex **2** crystallizes in monoclinic system with space group *P*n. X-ray structural analysis of complex revealed that the asymmetric unit (Fig. 5.5) contains two Cu(II) atoms, two deprotonated Schiff base $(L^2)^{2-}$, one $(tp)^{2-}$ anions and one lattice water molecule.

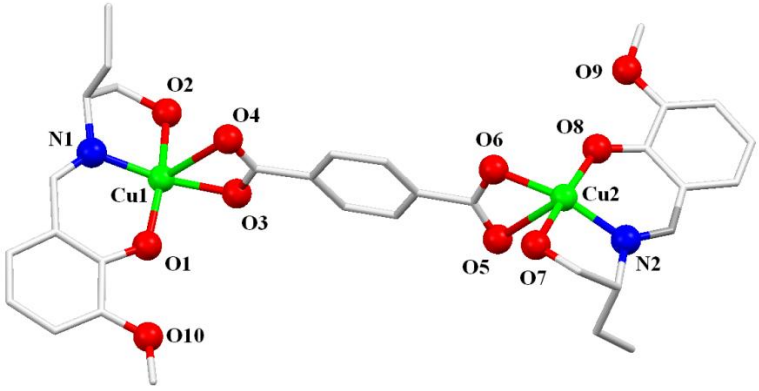

Fig. 5.5 Asymmetric unit of complex **2**.

The dinuclear copper units are connected through terephthalate ions forming 1D coordination polymers (Fig. 5.6). Both the copper atoms(Cu1 and Cu2) possess adistorted octahedral environment formed by a deprotonated tridentate (O, N, O) Schiff base ligand, and two oxygen atoms from one carboxylate group and another oxygen atom from other carboxylate group.

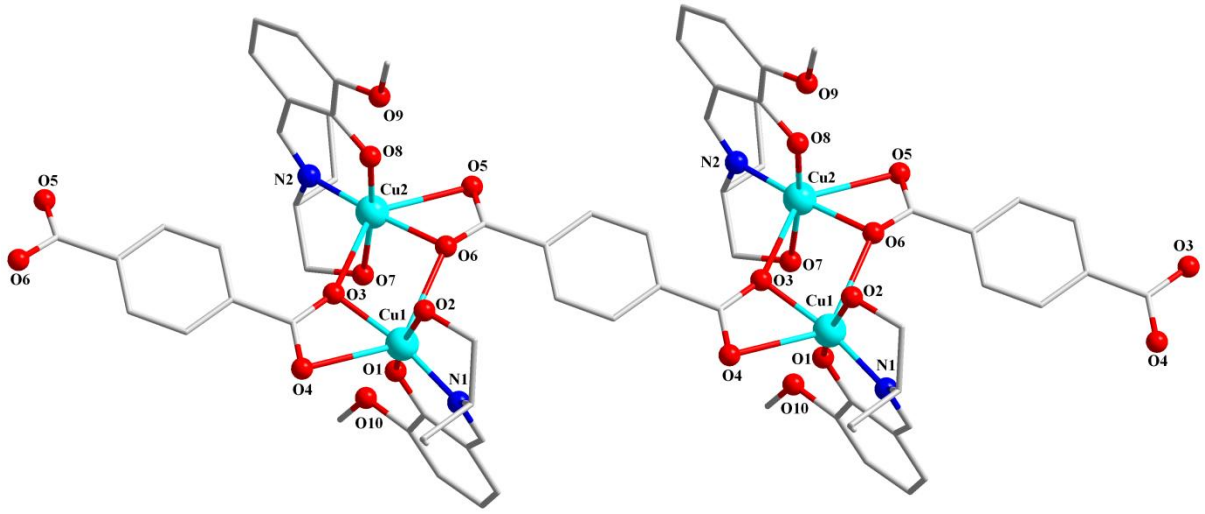

Fig. 5.6 The 1D polymeric structure of complex **2**. The lattice water molecule and hydrogen atoms have been omitted for clarity.

The square plane of the octahedron is formed by the three atom donors from Schiff base (O1, O2, N1 for Cu1; O7, O8, N2 for Cu2) and one oxygen atom from carboxylate (O3 for Cu1; O6 for Cu2), whereas the apical positions are occupied by two oxygen atoms from carboxylate groups, of which one of a symmetry related tp (O4, O6" for Cu1; O3', O5 for Cu2). The larger distortion of the octahedron is represented by the trans angles of axial legand, i.e., O4-Cu1-O6a of 132.56(9)° and O3b-Cu2-O5 of 134.95(10)°. The four equatorial donor atoms are almost coplanar, with a maximum deviation of -0.0094 Å for Cu1, and 0.0122 Å for Cu2 from the respective mean plane. The coordination environments of the two copper(II) atoms are slightly different due to different bond lengths and angles. The Cu-O bond lengths vary from 1.899(3) Å to 2.687(3) Å, whereas Cu-N ones are 1.926(3) and 1.923(3) Å. The distance between two copper atoms is 3.529(11) Å, indicating no interaction between the two metal centers. The Cu-O-Cu bridge angles are 97.77(102) and 102.39(107)°. The packing diagram shows that complex **3** exists as 1D polymeric chain through terephthalate linkage with metals spaced by 10.834 Å (Fig. 5.6) and these 1D chains are again interconnected through three different types C-H…π

interactions (C-H…Cg, 2.92, 2.74 and 3.20 Å) (Table 5.4) to form a 3D supramolecular architecture (Figs. 5.7-5.9).

Table 5.4 C-H…π interactions in complex **2**

C-H	Cg(J)	H···Cg (Å)	X-H···Cg (º)	X···Cg (Å)
C(16) -H(16C)	Cg(3)→ C(22)-C(23)-C(24)-C(25)-C(26)-C(27)	2.92	133	3.647(8)
C(18)-H(18)	Cg(2)→ C(10)-C(11)-C(12)-C(13)-C(14)-C(15)	2.74	168	3.705(6)
C(29)-H(29C)	Cg(2)→ C(10)-C(11)-C(12)-C(13)-C(14)-C(15)	3.20	118	3.746(57)

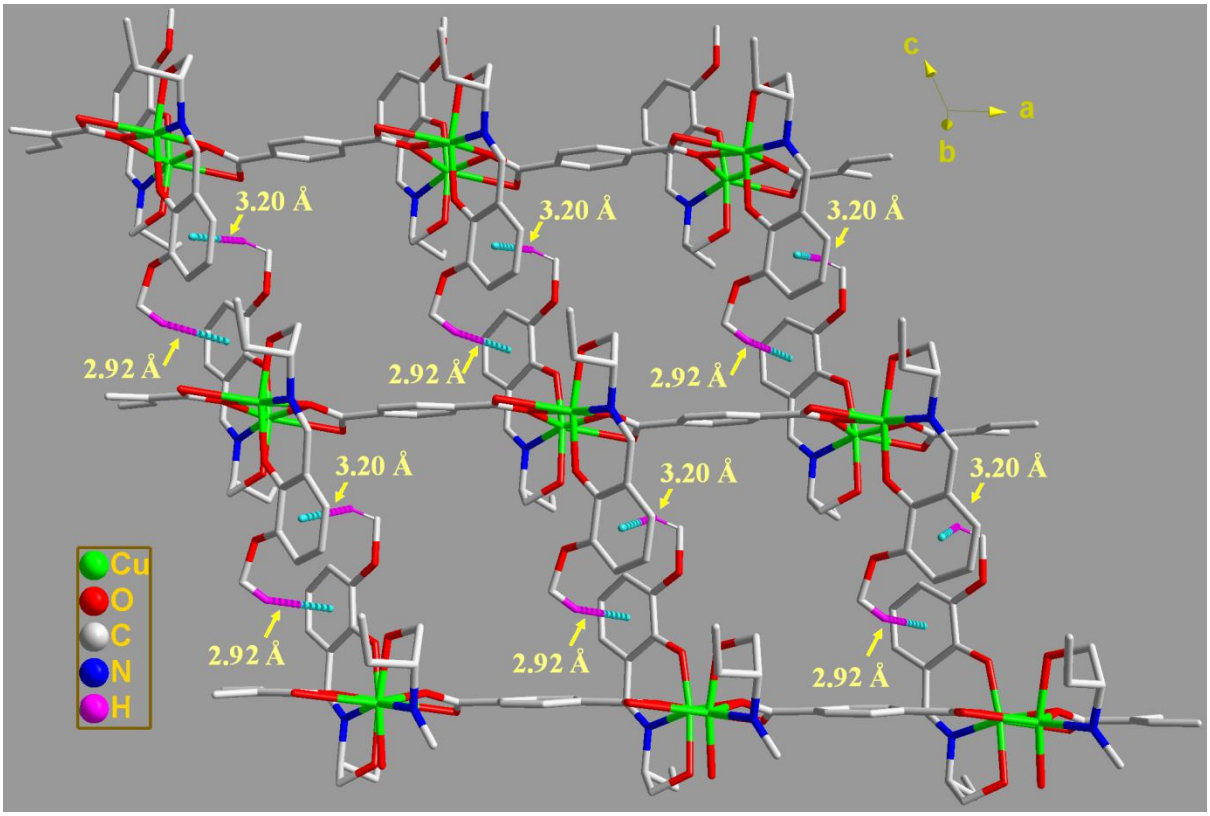

Fig. 5.7 2D supramolecular sheet formed by the C-H…π interaction in complex **2**.

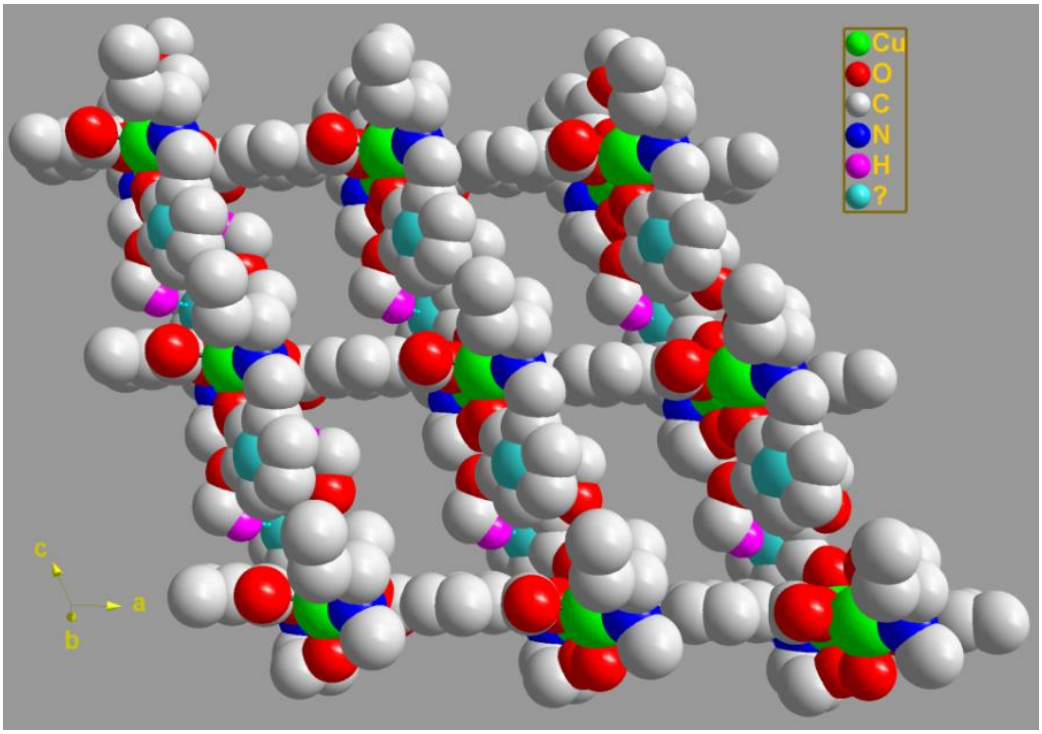

Fig. 5.8 2D supramolecular sheet formed by the C-H…π interaction (in space fill model).

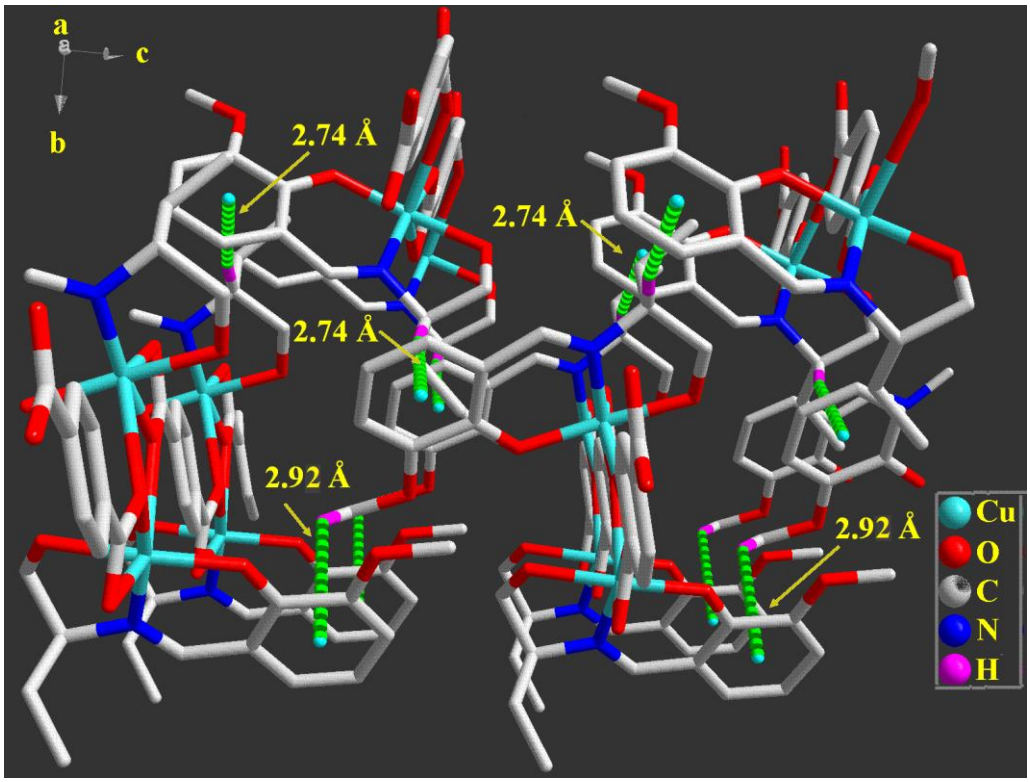

Fig. 5.9 3D supramolecular network formed by the C-H…π interaction.

Table 5.5 Selected bond lengths (Å) and angles (°) for **2**.

Bond lengths		Bond angles			
Cu(1)-O(1)	1.906(3)	O(1)-Cu(1)-O(2)	168.79(14)	O(5)-Cu(2)-O(6)	56.00(11)
Cu(1)-O(2)	2.007(3)	O(1)-Cu(1)-O(3)	91.87(12)	O(5)-Cu(2)-O(7)	88.59(13)
Cu(1)-O(3)	1.957(2)	O(1)-Cu(1)-O(4)	102.66(13)	O(5)-Cu(2)-O(8)	99.82(13)
Cu(1)-O(4)	2.555(3)	O(1)-Cu(1)-N(1)	93.30(12)	O(3_a) -Cu(2)-O(5)	134.95(10)
Cu(1)-N(1)	1.926(3)	O(1)-Cu(1)-O(6_b)	84.83(10)	O(5)-Cu(2)-N(2)	112.14(13)
Cu(1)-O(6)a	2.687(3)	O(2)-Cu(1)-O(3)	94.04(12)	O(6)-Cu(2)-O(7)	90.65(12)
Cu(2)-O(5)	2.572(4)	O(2)-Cu(1)-O(4)	88.55(12)	O(6)-Cu(2)-O(8)	93.88(12)
Cu(2)-O(6)	1.953(2)	O(2)-Cu(1)-N(1)	82.86(12)	O(3_a)-Cu(2)-O(6)	80.19(11)
Cu(2)-O(7)	2.023(3)	O(2)-Cu(1)-O(6_b)	87.29(10)	O(6)-Cu(2)-N(2)	166.86(14)
Cu(2)-O(8)	1.899(3)	O(3)-Cu(1)-O(4)	56.67(11)	O(7)-Cu(2)-O(8)	171.59(13)
Cu(2)-O(3)b	2.546(3)	O(3)-Cu(1)-N(1)	167.57(13)	O(3_a) -Cu(2)-O(7)	81.31(10)
Cu(2)-N(2)	1.923(3)	O(3)-Cu(1)-O(6_b)	76.54(11)	O(7)-Cu(2)-N(2)	82.97(12)
		O(4)-Cu(1)-N(1)	111.09(11)	O(3_a)-Cu(2)-O(8)	92.47(11)
		O(4)-Cu(1)-O(6_b)	132.56(10)	O(8)-Cu(2)-N(2)	93.95(12)
		O(6_b)-Cu(1)-N(1)	115.18(12)	O(3_a)-Cu(2)-N(2)	109.99(13)

Symmetry operations:atom at a = 1+x, y, z;b = x-1, y, z.

5.3.2 Electronic absorption and emission spectra of complexes

The spectrum of **1** (Fig. 5.10) shows significant transitions 222 ($\varepsilon \sim 4.98\times10^4\ M^{-1}cm^{-1}$), 238 ($\varepsilon \sim 4.40\times10^4\ M^{-1}cm^{-1}$), 268 ($\varepsilon \sim 2.72\times10^4\ M^{-1}cm^{-1}$) and 366 ($\varepsilon \sim 1.03\times10^4\ M^{-1}cm^{-1}$) nm. On the other hand the electronic spectrum of **2**, shows three significant transitions (Fig. 5.11) at 232 nm ($\varepsilon \sim 1.29\times 10^5$ liter mole^{-1} cm^{-1}), 273 nm ($\varepsilon \sim 5.4\times 10^4$ liter mole^{-1} cm^{-1}), and 370 nm ($\varepsilon \sim 1.0\times 10^4$ liter mole^{-1} cm^{-1}).

Study of the luminescence property (Fig. 5.10) of complex **1** at room temperature shows red shifted emission (Table 5.6) with large Stokes shifts (44 - 96 nm). On excitation at 366 nm complex **1** exhibits emission at 410, 433 and 462 nm in methanol with a fluorescence quantum yield Φ_s = 0.257. On the other hand on excitation at 370 nm complex **2** exhibits luminescence bands at 448 nm (Fig. 5.11) with a quantum yield (Φ_s) = 0.37.

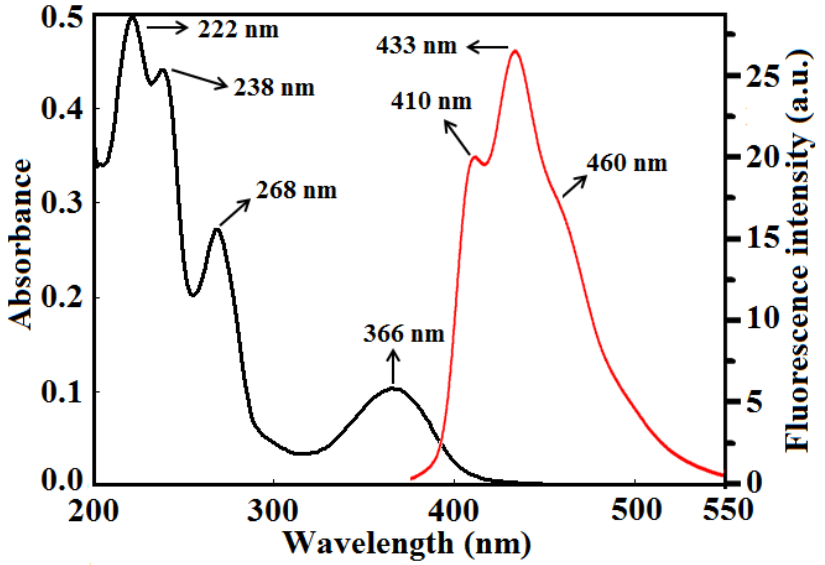

Fig. 5.10 Electronic absorption and emission spectra of complex **1**.

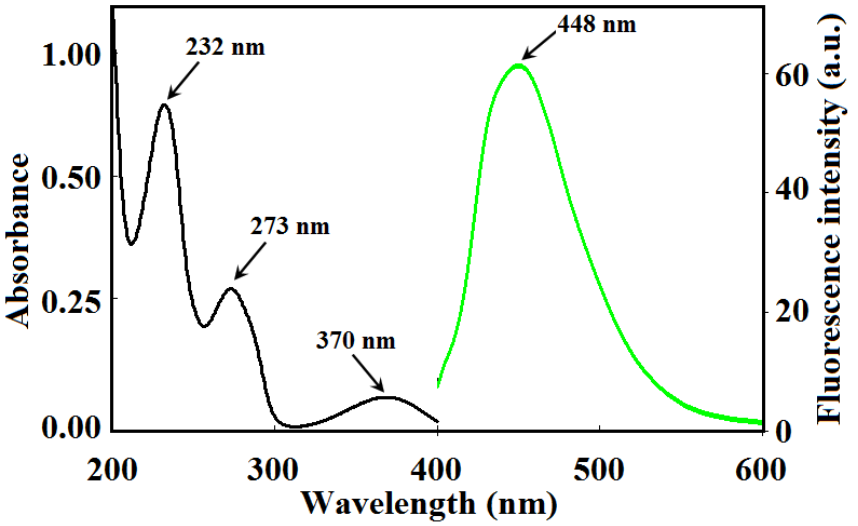

Fig. 5.11 Electronic absorption and emission spectra of complex **2**.

Table 5.6 Photo-physical parameters of complexes.

	Absorption λ (nm), ε_{exp} ($M^{-1}cm^{-1}$)	Emission λ_{em}(nm)	$\Delta\nu^{[a]}$ (nm)	Φ_s
1	222 (0.498×10^5), 238 (0.440×10^5), 268 (0.272×10^5), **366** (0.103×10^5)	410, 433, 462	44, 67, 96	0.257
2	232(1.29×10^5), 273 (5.4×10^4), **370** (1.0×10^4)	448	78	0.37

Bold number indicates the excitation wavelengths.[a]Stoke shift

5.3.3 Protein binding studies

Serum albumin binding study using electronic absorption spectroscopy

The changes in the electronic absorption spectra of bovine serum albumin (BSA) (3 ml, 8.214 µM aqueous solution) and human serum albumin (HSA) (3 ml, 3.109 µM aqueous solution) in the presence of different concentrations of complex **1** and **2** (using HEPES buffer, pH 7.2) at 300 K temperature are shown in Fig. 5.12 and Fig. 5.13, respectively.

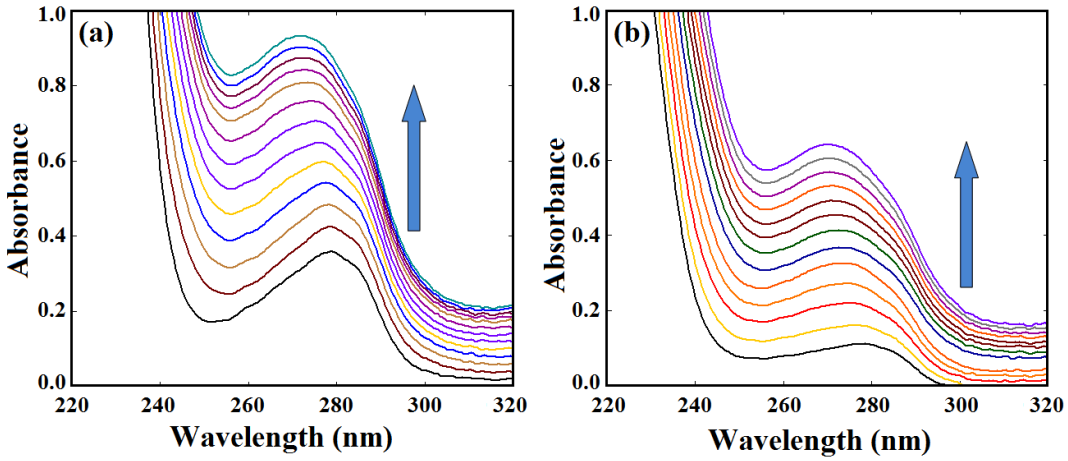

Fig. 5.12 Change of electronic absorption spectra of BSA (**a**) and HSA (**b**) upon gradual addition of complex **1** at temperature 300 K.

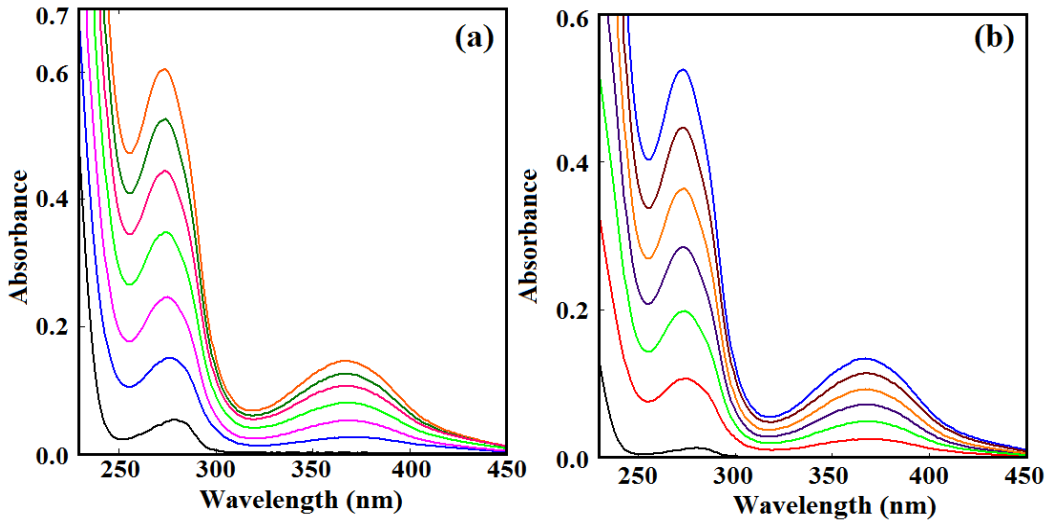

Fig. 5.13 Change of electronic absorption spectra of BSA (**a**) and HSA (**b**) upon gradual addition of complex **2** at temperature 300 K.

The UV-vis spectral band of serum albumins at 280 nm is blue shifted in presence of complexes **1** (6 nm for BSA, 7 nm for HSA) and 2 (5 nm for BSA, 6 nm for HSA). A bathochromic shift at 280 nm confirms the ground state association of complexes with serum albumins. The apparent association constants (K_{app}) were calculated adopting the following equation

$$\frac{1}{(A_{obs} - A_0)} = \frac{1}{(A_c - A_0)} + \frac{1}{K_{app}\,(A_c - A_0)[complex]}$$

where A_{obs} is the observed absorbance (at 280 nm) of the solution containing different concentrations of the complex, A_0 is the absorbance of serum albumin only and A_c is the absorbance of serum albumin with complexes. From the plot (Fig. 5.14 and Fig. 5.15) of $1/(A_{obs}-A_0)$ versus 1/[complex] the values of apparent association constants were calculated and the calculated values are 1.34×10^4 (for 1-BSA), 1.81×10^4 (for 1-HSA), 1.21×10^3 (for **2**-BSA) and 0.94×10^3 $Lmol^{-1}$ (for **2**-HSA) (Table 5.7).

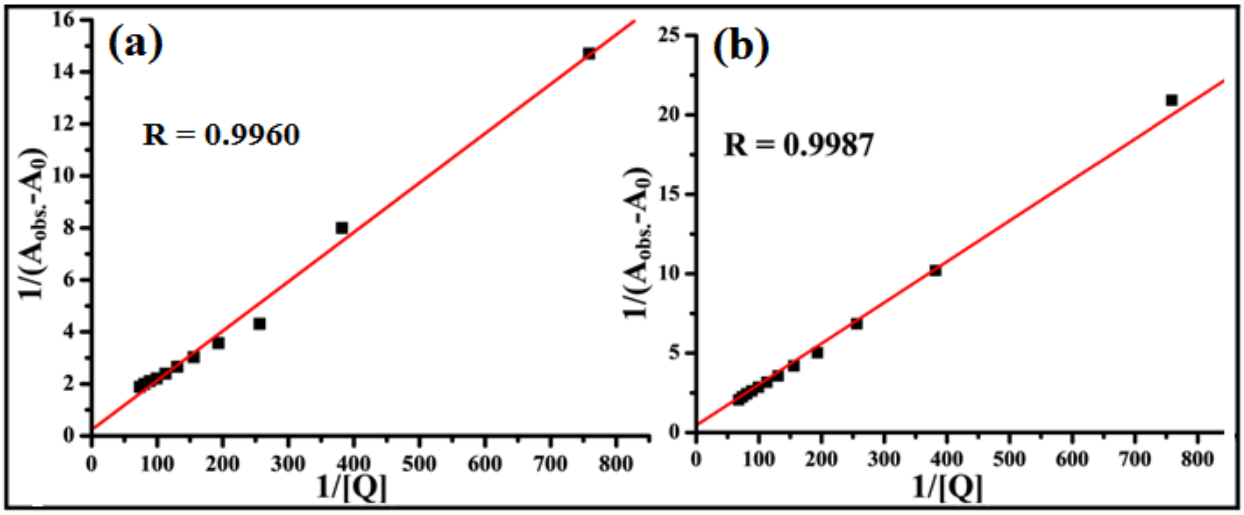

Fig. 5.14 Plot of $1/(A_{obs} - A_0)$ versus reciprocal of complex **1** concentration for titration with BSA (**a**) and HSA (**b**) at 300 K.

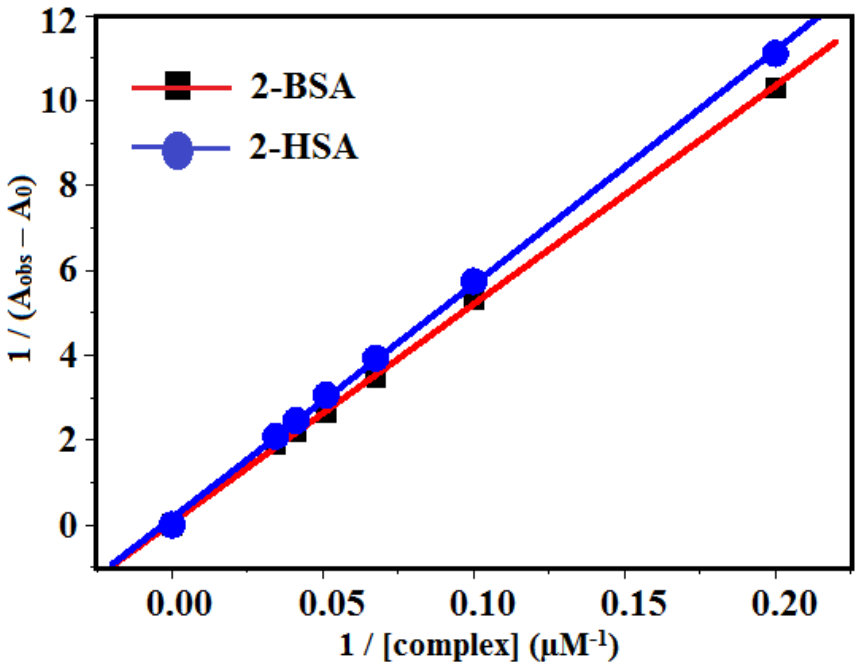

Fig. 5.15 Plot of $1/(A_{obs} - A_0)$ versus reciprocal of complex **2** concentration for titration with BSA and HSA at 300 K.

Table 5.7 Apparent binding constant (K_a), Stern-Volmer constant (K_{sv}), quenching constant (k_q), binding constant (K_b) and number of binding sites (n) for the interaction of complexes **1** and **2** with of BSA and HSA.

	Complexes	K_{sv} (L mol^{-1})	k_q(L $mol^{-1}s^{-1}$)	K_b (L mol^{-1})	n	K_a (L mol^{-1})
BSA	**1**	2.0933×10^5	4.1866×10^{13}	7.8324×10^5	1.34	1.3468×10^4
	2	1.42×10^5	2.84×10^{13}	1.03×10^5	1.13	1.21×10^3
HSA	**1**	1.397×10^5	2.794×10^{13}	7.5557×10^5	1.14	1.8153×10^4
	2	5.78×10^4	1.15×10^{13}	7.94×10^4	0.87	0.94×10^3

Fluorescence quenching of serum albumins by complexes

The binding interactions of serum albumins with the complexes were studied by fluorescence spectroscopy. On excitation at 280 nm, an aqueous solution (pH 7.2, HEPES buffer) of the serum albumins (BSA/HSA) exhibit luminescence at 340 nm. The changes in the fluorescence spectra of serum albumins upon addition of increasing concentrations (0 - 11.269 μM) of complex **1** and complex **2** are shown in Fig. 5.16 and Fig. 5.17, respectively.

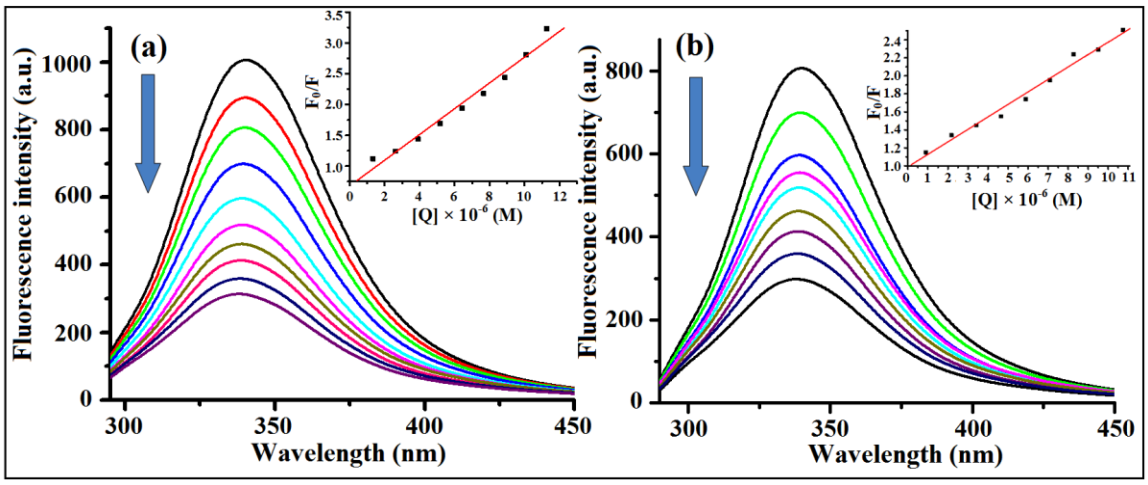

Fig. 5.16 Fluorescence quenching curves of BSA (a) and HSA (b) in the presence of increasing amounts of complex **1**(0-11.269 µM). Arrow shows that the emission intensity changes upon increasing complex concentration (Inset: Stern-Volmer plot of the fluorescence titration).

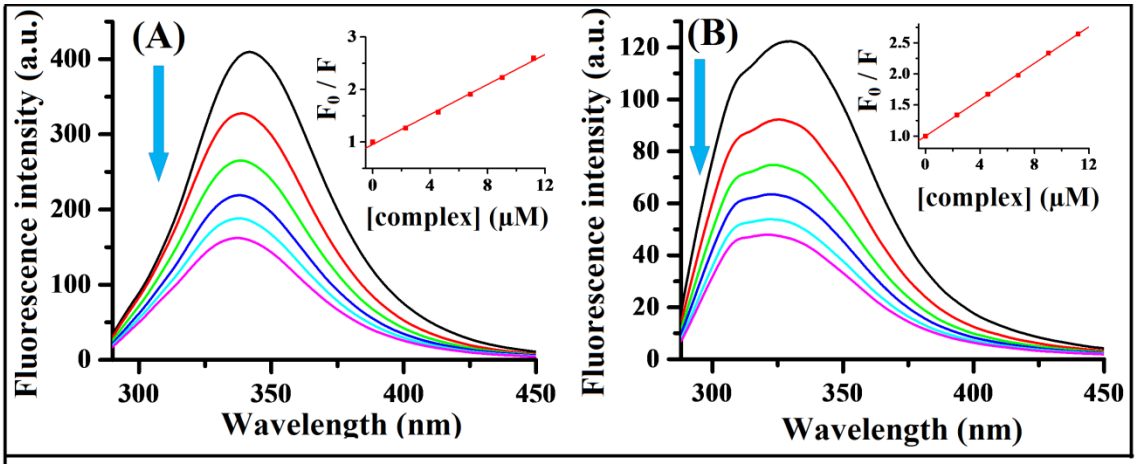

Fig. 5.17 Emission spectrum of BSA (A) and HSA (B) in the presence of increasing amounts of complexes **2** (0-11.269 µM). Arrow shows that the emission intensity changes upon increasing complex concentration (Inset: Stern-Volmer plot of the fluorescence titration).

A significant decrease in the fluorescence intensity (up to 68.67 % quenching with a 3 nm blue shift for BSA, and up to 63.19 % quenching with a 2 nm blue shift for HSA) was observed at 340 nm upon gradual addition of 20 µL, 0.199 µM of an aqueous solution of complex **1**. Whereas the fluorescence intensity of serum albumins quenched with a small hypsochromic shift (up to 65.36 % quenching with a 3 nm blue shift for BSA, and up to 62.16 % quenching with a 6 nm blue

shift for HSA) at 340 nm upon gradual addition of 20 µL, 0.3475 mm solution of an aqueous solution of complex **2**.

This hypochromicity in the spectra reveals that the complexes bind with serum albumins. From the Stern-Volmer equation [5.23] a linear relationship were obtained for the titration of serum albumins, using complexes **1** and **2** as quencher (inset of Fig. 5.16 and Fig. 5.17).

The calculated values of Stern-Volmer constants (K_{SV}) and quenching rate constant (K_q) for BSA binding are $K_{sv} = 2.09 \times 10^5$, $k_q = 4.18 \times 10^{13}$ for **1** and $K_{SV} = 1.42\times10^5$, $K_q = 2.84 \times10^{13}$ for **2**. Whereas for HSA binding $K_{sv} = 1.39 \times 10^5$, $k_q = 2.79 \times 10^{13}$ for **1** and $K_{SV} = 5.78\times10^4$, $K_q = 1.15\times10^{13}$ for **2** (Table 7). The values of K_{sv} and k_q indicate that both the complexes have good fluorescence quenching ability. The UV-vis absorption spectra of BSA/HSA show significant changes on addition of complexes, this phenomenon evidences the existence of static interaction between BSA/HSA and complexes **1-2**. The presence of a static interaction is again supported by the very high values of k_q ($\sim 10^{13}$ L mol^{-1} s^{-1}). These values are much greater than the maximum values (2×10^{10} L mol^{-1} s^{-1}) of the diffusion collision quenching rate constant of various kind of fluorescence quenchers for biopolymers [5.41]. The binding constants (K_b) for the interaction of serum albumins with complexes and the number of binding sites (n) per albumin were also calculated using the Scatchard equation. The plot of $\log\frac{(F_o-F)}{F}$ versus log[complex] gives a straight line (Figs. 5.18-5.19) with n and $\log K_b$ as slope and intercept, respectively. The calculated values of k_b and n are given in Table 5.7. Studies of the kinetics of interaction of serum albumins (BSA / HSA) with the Schiff base coordinated mononuclear copper(II) complexes are reported in literature [5.42, 5.43], but studies of the kinetics of interactions of BSA / HSA with polynuclear copper(II) compound are scarce.

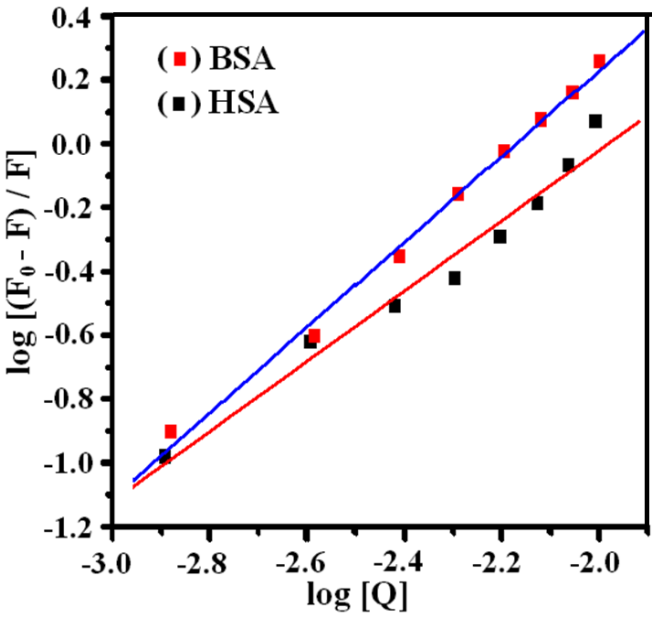

Fig. 5.18 Double-logarithm curves of BSA and HSA fluorescence quenching by complex **1**

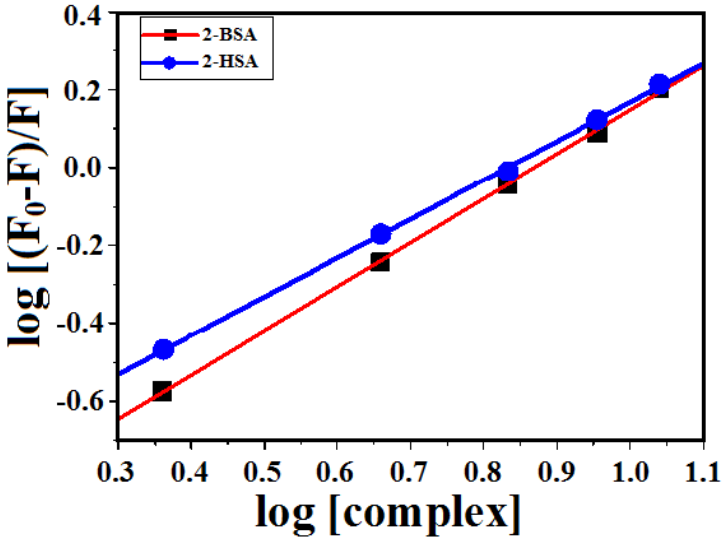

Fig. 5.19 Double-logarithm curves of BSA and HSA fluorescence quenching by complex **2**

5.3.4 DNA binding studies

Electronic absorption spectral titration

The intercalation between a compound and DNA [5.44] is evident by hypochromism in the electronic spectra of compound with or without red/blue shift upon gradually increasing the

concentration of DNA. On the contrary, a non-intercalative interaction between the compound and DNA is supported by hyperchromism in the absorption spectra of a compound with increasing concentration of DNA [5.45]. Figs. 5.20-5.21 display the change in the electronic absorption spectra of complexes **1-2** (0.199 µM aqueous solution) with increasing concentrations of CT-DNA (0-20.94 µM).

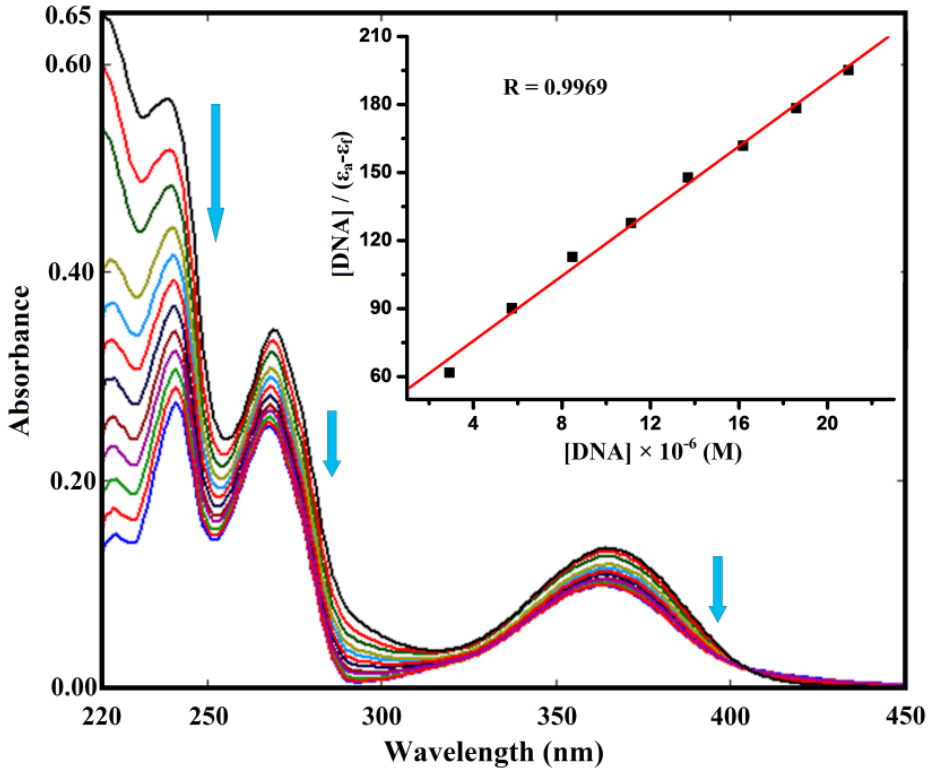

Fig. 5.20 Change of electronic absorption spectra of complex **1** upon gradual addition of aqueous solution of CT-DNA. Inset: Plot of [DNA] / (ε_a-ε_f) versus [DNA]. Arrows show the changes in absorbance with respect to an increase in the DNA concentration.

Hypochromism of about 48.14, 25.14, and 25.18% were observed for the spectral bands at 238, 268, and 366 nm, respectively for complex **1**. The bands at 238 and 268 nm showed hypochromism with a 2 nm red shift and a 1 nm blue shift, respectively, whereas no shifting was observed for at 366 nm.

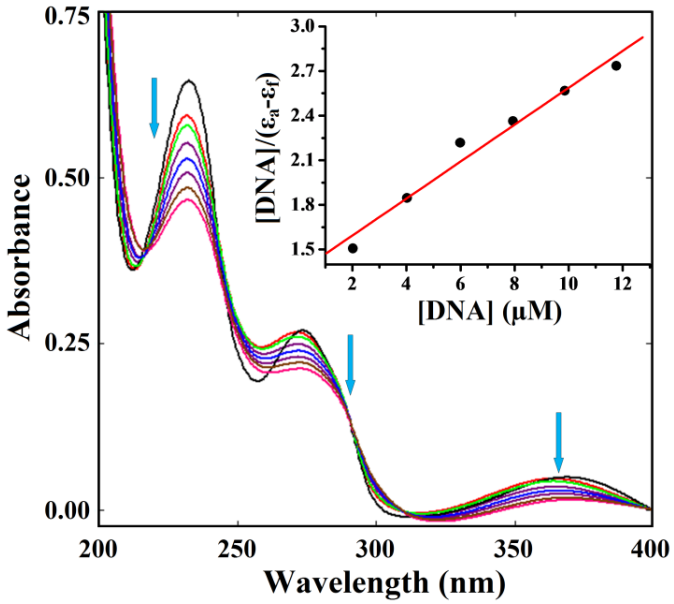

Fig. 5.21 Absorption titration spectra of complex **3** in the absence (black line) and presence (other lines) of CT-DNA to complex at room temperature. Inset: Plot of [DNA]/(ε_a-ε_f) versus [DNA]. Arrow shows the absorbance changes upon increasing CT-DNA concentration.

On the other hand hypochrmism of about 16.33 % was observed without any significant shift at 232 nm for complex **2**. These spectral changes indicate that both the complexes bind to the CT-DNA helix via intercalation. A plot of [DNA]/($\varepsilon_a - \varepsilon_f$) versus [DNA] (Figs. 5.20-5.21, inset) is a straight line with $\frac{1}{(\varepsilon_b - \varepsilon_f)}$ and $\frac{1}{K_{ib}(\varepsilon_b - \varepsilon_f)}$ as the slope and intercept, respectively. The values of the intrinsic binding constant (K_{ib}) were calculated from the ratio of the slope to the intercept and the calculated value of K_{ib} are 2.96×10^5 and 0.92×10^5 M^{-1} for complexes **1**-**2**, respectively.

Ethidium Bromide (EB) displacement studies

Ethidium bromide (EB) shows fluorescence with an orange color, when it exposed to ultra violet radiation. The intensity of the EB fluorescence increases around 20 fold in the presence of CT-DNA due to strong intercalation of the planar ethidium bromide phenanthridium ring between adjacent base pair of the double helix [5.43, 5.46]. CT-DNA bounded EB shows emission at 612 nm on excitation at 500 nm. Addition of a compound, which is capable to interact with CT-

DNA, to a solution of a mixture of EB-(CT-DNA) results in the quenching of EB-(CT-DNA) fluorescence intensity. The quenching of the fluorescence occurs due to a decrease in the number of binding sites on the CT-DNA available for EB. The fluorescence quenching observed in the presence of a compound may be used to study intercalation between CT-DNA and this compound. Fig. 5.22 and Fig. 5.23 show the change of the fluorescence spectra of CT-DNA bonded EB upon gradual addition of complex **1** and complex **2**, respectively.

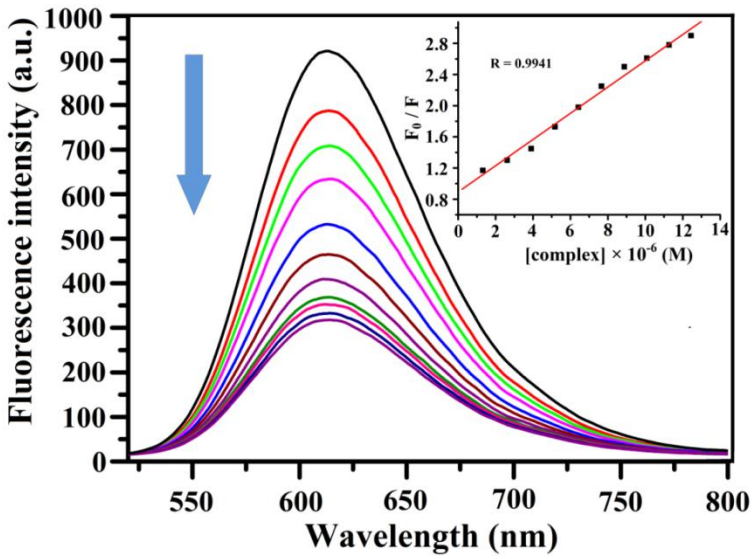

Fig. 5.22 Fluorescence quenching curves of EB bound to CT-DNA in the presence of complex **1**. Inset: Stern-Volmer plot of fluorescence titration.

Hypochromism (up to 65.58 % for **1** and 51 % for **2** of the initial fluorescence intensity) in the presence of complexes suggests that the EB molecules are displaced from the CT-DNA binding sites by complexes [5.43, 5.46, 5.47]. From the Stern-Volmer plot [5.23] (insets of Figs. 5.22-5.23) the binding constant (K_{sv}) were calculated and calculated values are 1.701×10^5 and 0.75×10^5 M^{-1} for **1** and **2**, respectively.

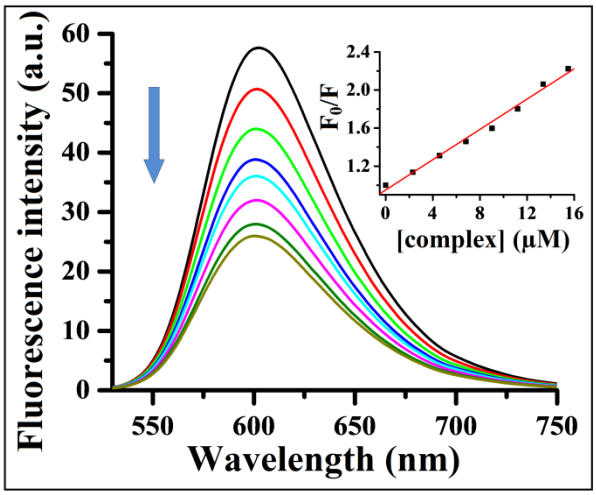

Fig. 5.23 Fluorescence quenching curves of EB bound to CT-DNA in the presence of complex **2**. Inset: Stern-Volmer plot of fluorescence titration.

Although many authors have reported binding behavior of Schiff base coordinated mononuclear first-row transition metal coordination compounds [5.42, 5.43] with CT-DNA, but the studies are quite rare for polynuclear copper complexes. Table 5.8 shows the binding parameters of CT-DNA with polynuclear copper(II) compounds [5.48, 5.49]. The K_{ib} value for complex **1** is slightly higher than the reported values, whereas, K_{ib} value for complex **1** and K_{sv} values for both the complexes are comparable to the reported values.

Table 5.8 CT-DNA / BSA binding parameters of polynuclear Cu(II) compounds.

Compound	DNA binding		Protein binding			Ref.
	K_{ib} (10^5 M^{-1})	K_{sv} (10^4 M^{-1})	K_{sv} (10^5 M^{-1})	K_b (10^5 M^{-1})	n	
$\{[Cu_2(HL)_2(fum)]\cdot(H_2O)\cdot(MeOH)\}_n$	2.96	17.1	2.093	7.8324	1.34	this work
$\{[Cu_2(L^1)(bipy)]\cdot(ClO_4)_2\cdot CH_3CN\}_n$	0.72	-	-	-		5.48
$\{[Cu_2(L^2)(bipy)]\cdot(ClO_4)_2\cdot H_2O\}_n$	2.1	-	-	-		5.48
$[Cu_2(L^3)_2(H_2O)]_n$	0.049	-	-	-		5.49
$\{[Cu_2(L^4)_2(H_2O)]\ H_2O\}_n$	0.087	-	-	-		5.49

H_2L^1, [2 + 2] condensation product of 1,3-diaminopropane with 2,6-diformyl- 4-methylphenol; H_2L^2, [2 + 2] condensation product of 1,3-diaminopropane with 2,6-diformyl-4-fluorophenol; H_2L^3, a Schiff base derived from condensation of N-(2-hydroxybenzaldehyde) with L-methionine. H_2L^4 is reduced form of H_2L^3.

5.3.5 Magnetic properties

Temperature-dependent magnetic susceptibility measurements on a polycrystalline sample of complexes **1-2** were carried out in the temperature range 1.9-300 K. The plot of $\chi_M T$ versus T curve for complex **1** is shown in Fig. 5.24, where χ_M is the molar magnetic susceptibility and T is the absolute temperature. The $\chi_M T$ value measured at room temperature, of 0.84 cm^3Kmol^{-1} is slightly higher than the expected value for two uncoupled S = ½ spins, assuming g = 2 (0.75 cm^3Kmol^{-1}). Upon cooling, $\chi_M T$ varies smoothly and finally drops to zero, reaching a plateau at temperatures below 10 K. The behavior displayed by complex **1** confirms the presence of an overall antiferromagnetic interaction in the complex. The experimental magnetic data were simulated with the MAGPACK program [5.50]. The model assumed the crystallographic equivalence of the two Cu(II) ions within the dinuclear unit by assigning one single g value for both ions. Additionally, the interaction between Cu_2 units through the fumarate bridge was considered negligible, since it is expected to be between one and two orders of magnitude weaker than the interaction with in the Cu_2 dinuclear unit [5.51]. For the spin Hamiltonian $H = -JS_1S_2$, $S_1 = S_2 = S_{Cu}$, a good agreement between the experimental and simulated curves for **1** was found by using the following parameters: g_{Cu}= 2.20 and $J_{Cu\text{-}Cu}$= –60 cm^{-1}. Temperature-independent paramagnetism (TIP) was considered equal to 150 × 10^{-6} cm^3mol^{-1}. The simulated curve is represented together with the experimental values in Fig. 5.24. The antiferromagnetic coupling in complex **1** can be understood in the light of orbital symmetry considerations. The two copper(II) ions in the asymmetric unit are penta-coordinated and the two square pyramids formed share one base-to-apex edge with parallel basal planes [5.52]. The unpaired electron in each Cu(II) ion resides mainly in the basal $d_{x^2-y^2}$ orbital.

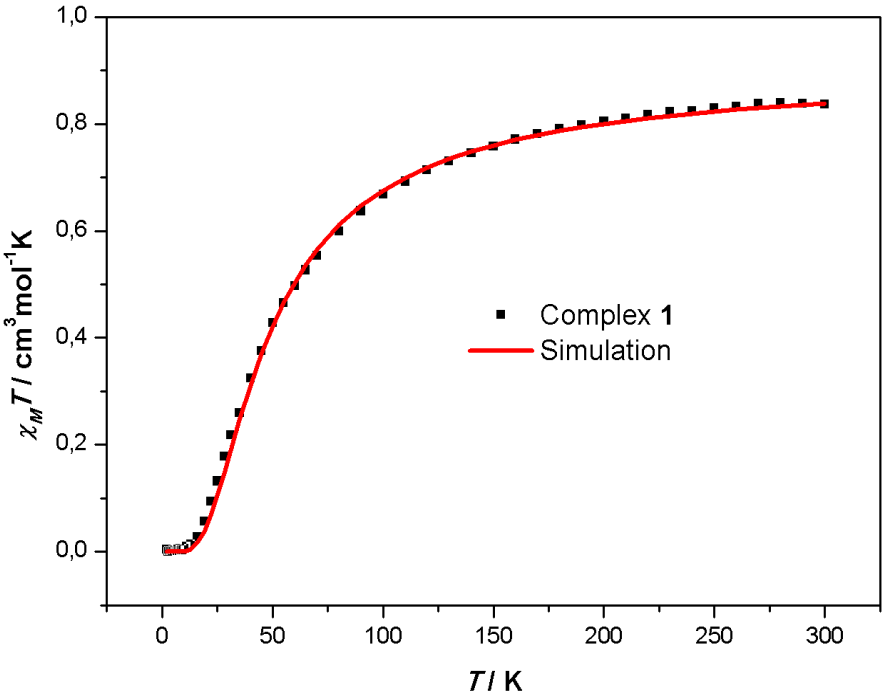

Fig. 5.24 $\chi_M T$ versus T plot for complex **1** (solid line represents the best fit).

Thus, the two parallel magnetic orbitals are orthogonally connected through an axial position occupied by the monodentate fumarate bridge. If a perfect square-pyramid environment ($\tau = 0$) is assumed for both Cu(II) ions, there would be no overlap between their magnetic orbitals, and consequently the magnetic interaction would be negligible or weakly ferromagnetic. However, in complex **1** only Cu(2) shows a local geometry close to that of a perfect square-pyramid (τ = 0.013), while Cu(1) exhibits a larger distortion (τ = 0.128). Such distortion is responsible for an increase of the overlap between $d_{x^2-y^2}$ magnetic orbitals in the asymmetric unit, and as a result a moderate antiferromagnetic exchange operates between the two Cu(II) ions [5.53].

The $\chi_M T$ vs T curve for complex **2** is shown in Fig. 5.25. It shows a room temperature value of 0.81 cm^{3}mol^{-1}K, slightly higher than the value of 0.75 cm^{3}mol^{-1}K expected for two uncoupled S = ½ spins assuming g = 2. This value is maintained constant down to ca. 20 K, and below this

temperature the curve drops fast until a value of 0.62 $cm^3mol^{-1}K$ is reached at 2 K. The experimental data confirm the presence of a very weak antiferromagnetic interaction in the complex. Complex **2** consists of one dimensional polymeric chains formed by the linkage of the asymmetric dinuclear unit shown in Fig. 5.25. Neighbouring dinuclear units are bridged by terephthalate ions and thus long Cu···Cu inter-dinuclear distances of the order of 10 Å are measured, which predicts a negligible inter-dinuclear magnetic coupling within the chains. By assuming this hypothesis, the analysis of the magnetic data of complex **3** can be carried out by using a simple dinuclear model with the anisotropic Hamiltonian of type: $H = -J\,(S_1S_2)$, where J describes the magnetic exchange operating between the two Cu(II) ions in the asymmetric dinuclear unit. The $\chi_M T$ vs T curve of complex **2** was fitted with the PHI program [5.54]. A single g value was considered in the analysis and the temperature-independent paramagnetism (TIP) was considered equal to 60×10^{-6} cm^3mol^{-1}. A good agreement with the experimental curve was found with the following parameters: $g = 2.08$ and $J = -0.5$ cm^{-1}. The fitted curve is represented together with the experimental one in Fig. 5.25. The results of the fit confirm the very weak antiferromagnetic coupling between Cu(II) ions in the dinuclear unit, which might be expected considering that the two Cu(II) ions are bridged by two carboxylate groups with axial non-magnetic orbitals involved in both exchange pathways. This situation drastically diminishes the overlap between magnetic orbitals of the two ions making the exchange very weak or almost negligible, as experimentally observed in complex **2**.

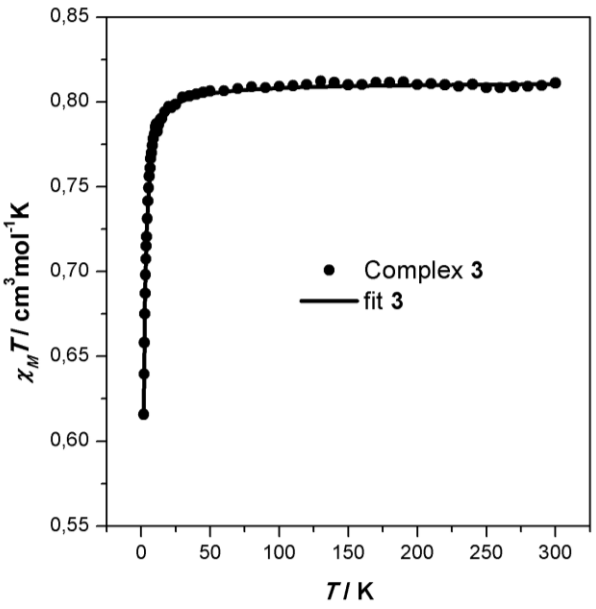

Fig. 5.25 Thermal dependence of the $\chi_M T$ for complex **2**. The straight line represents the fit obtained considering a Cu(II) dinuclear model and using the Hamiltonian and parameters mentioned in the text.

5.4 Conclusion

In summary, we have presented here the synthesis, crystal structure, low-temperature magnetic behavior and study of the interactions with BSA / HSA and CT-DNA of two novel carboxylate bridged copper(II) compounds using O,N,O donor chelating ligand. The copper(II)-Schiff base complexes in combination with linear rigid carboxylate ligand, generates 1D polymeric chain. The CT-DNA and protein binding of the compounds were investigated using electronic absorption and fluorescence spectroscopic techniques. Both the complex are rare example of polynuclear copper(II) compounds which are interacts with CT-DNA/serum albumin. A comparison of the kinetic parameters of interaction of reported polynuclear copper(II) compounds with CT-DNA reveals that complex **1** interacts slightly more strongly than the reported polynuclear copper(II) compounds. The experimental magnetic data of both the

compounds were fitted with a pseudo-dinuclear copper(II) model and the results show the presence of an antiferromagnetic interaction.